

L2V-CoT: Cross-Modal Transfer of Chain-of-Thought Reasoning via Latent Intervention

Yuliang Zhan*, Xinyu Tang*, Han Wan, Jian Li, Ji-Rong Wen, Hao Sun†

Gaoling School of Artificial Intelligence, Renmin University of China, Beijing, China
 {zhanyuliang, xinyun_tang, wanhan2001, lijian2022, jrwen, haosun}@ruc.edu.cn

Abstract

Recently, Chain-of-Thought (CoT) reasoning has significantly enhanced the capabilities of large language models (LLMs), but Vision-Language Models (VLMs) still struggle with multi-step reasoning tasks due to limited multimodal reasoning data. To bridge this gap, researchers have explored methods to transfer CoT reasoning from LLMs to VLMs. However, existing approaches either need high training costs or require architectural alignment. In this paper, we use Linear Artificial Tomography (LAT) to empirically show that LLMs and VLMs share similar low-frequency latent representations of CoT reasoning despite architectural differences. Based on this insight, we propose **L2V-CoT**, a novel training-free latent intervention approach that transfers CoT reasoning from LLMs to VLMs. **L2V-CoT** extracts and resamples low-frequency CoT representations from LLMs in the frequency domain, enabling dimension matching and latent injection into VLMs during inference to enhance reasoning capabilities. Extensive experiments demonstrate that our approach consistently outperforms training-free baselines and even surpasses supervised methods.

Introduction

Recently, reasoning models have achieved significant advancements in tackling a wide range of complex tasks (OpenAI 2024; Wang et al. 2025a; Guo et al. 2025; Wang et al. 2025b). A crucial factor contributing to this success is the Chain-of-Thought (CoT) method, which allows large language models (LLMs) to decompose complex problems into a sequence of intermediate reasoning steps (Xia et al. 2024). This approach has significantly improved their reasoning and decision-making capabilities (Zhang et al. 2025). In contrast, although Vision-Language Models (VLMs) have shown impressive results on tasks such as visual question answering (Hartsock and Rasool 2024) and image captioning (Kim et al. 2024; Li et al. 2025b), they still struggle with tasks that require multi-step reasoning, such as chart and geometric analysis (Cheng et al. 2025; Zhang et al. 2024). This problem is primarily attributed to the scarcity of multimodal reasoning data, as generating such data is both resource-intensive and time-consuming (Liu et al. 2025).

*These authors contributed equally.

†Corresponding author.

Copyright © 2026, Association for the Advancement of Artificial Intelligence (www.aaai.org). All rights reserved.

To address this problem, recent studies have explored ways to transfer reasoning capabilities from LLMs to VLMs. Virgo (Du et al. 2025) enables cross-modal reasoning transfer by training VLMs on large amounts of textual Chain-of-Thought (CoT) data. However, this approach is hindered by high training costs and limited generalization ability. To overcome this limitation, existing studies transfer reasoning capabilities from LLM to VLM through model merging (Chen et al. 2025; Zhan et al. 2024). Although this method achieves effective transfer, its applicability is limited to scenarios where the VLM and the source LLM are architecturally aligned. However, in real-world scenarios, the LLM backbone of VLM is not always aligned with the strong text reasoning model, which limits the upper bound of reasoning capabilities that can be transferred from LLMs to VLMs. This raises a practical challenge: How can we transfer reasoning abilities from LLMs to VLMs across **different architectures**?

Inspired by Contrast-Consistent Search (Burns et al. 2022), which suggests that model capabilities can be captured and manipulated through linear transformations, we explore the possibility of transferring reasoning capabilities across different model architectures. However, since models with different modalities often have distinct internal structures, it remains unclear whether the internal reasoning patterns encoded in one modality can be effectively interpreted, aligned, and transferred to another modality.

To further analyze reasoning capabilities across models of different modalities, we apply Linear Artificial Tomography (LAT) (Zou et al. 2023), a representation reading method that extracts latent states with contrastive inputs, to examine the latent representations of them. The findings of our analysis reveal that: (1) The **low-frequency components** of VLM’s CoT direction representations, derived from linear modeling of CoT and Non-CoT representations, can activate its reasoning ability. In contrast, the high-frequency components do not help. (2) These low-frequency representations have a **similar distribution** to those of LLMs. The observation suggests a consistent structural alignment in the latent space across modalities, which enables effective cross-modal transfer of reasoning ability.

Based on these insights, we propose **Latent Intervention** for **LLM-to-VLM CoT Transfertion (L2V-CoT)**, a training-free latent intervention method that transfers the general

CoT reasoning capabilities of LLMs to VLMs. Specifically, we collect CoT and Non-CoT from LLMs to construct contrastive samples. These samples are then encoded by the reasoning LLM to obtain CoT direction representations. However, representations derived from different architectures often encounter the dimension mismatch problem. To address this, we apply low-pass filtering to the CoT direction representations from the LLM to preserve essential CoT information. Then, we perform resampling in the frequency domain to match the dimension. These resampled representations are injected into the VLM via latent intervention during inference, thereby implicitly enhancing its reasoning ability. As a training-free and model-agnostic method, L2V-CoT enables efficient transfer the reasoning capabilities of LLMs to VLMs. To evaluate its effectiveness, we conduct experiments on multiple visual reasoning benchmarks across diverse VLMs. The experimental results demonstrate that L2V-CoT consistently outperforms other training-free baselines and even surpasses some supervised approaches.

Our contributions can be summarized as follows:

- To our best knowledge, we are the first to leverage Linear Artificial Tomography to analyze the transferability of reasoning capabilities between LLMs and VLMs.
- We propose L2V-CoT, a novel training-free method that transfers the general CoT reasoning capability of LLMs to VLMs, thereby enhancing the reasoning ability of VLMs.
- Extensive experiments validate the effectiveness of our approach in transferring CoT reasoning across modalities.

Related Work

Multimodal Chain-of-Thought Reasoning. As CoT reasoning proves effective in LLMs, recent work has extended it to multimodal tasks (Chen et al. 2024b; Li et al. 2025a). Existing methods fall into two main categories: explicit and implicit methods, which are orthogonal and complementary in enhancing VLM reasoning (Wu et al. 2025). Explicit methods guide reasoning step-by-step via rewards or search without altering model states (Yao et al. 2024). In contrast, implicit methods improve reasoning by modifying internal states (Luo et al. 2025; Zhang et al. 2023). LlamaV-01 (Thawakar et al. 2025) learns from multimodal CoT data. Given the scarcity of visual CoT annotations, Virgo (Du et al. 2025) trains VLMs on textual CoT data (Du et al. 2025). Parameter merging methods further enable training-free transfer from LLMs to VLMs but are constrained to architecture-aligned models (Chen et al. 2025). Our method, L2V-CoT, belongs to the implicit category. It enables architecture-agnostic, training-free CoT transfer from LLMs to VLMs via latent intervention, offering a flexible and generalizable solution for multimodal reasoning.

Activation engineering. Activation engineering modifies a model’s latent states for two main purposes: (1) understanding internal mechanisms and (2) controlling behavior (Zou et al. 2023). It uses representation reading to identify latent states tied to high-level concepts, supporting both interpretability and intervention. This method been applied to reducing hallucinations (Li et al. 2023; Tang et al. 2025a; Li et al. 2024) and adjusting sentiment (Tigges et al. 2024).

While recent work has explored using activation engineering for capability transfer within the model (Tang et al. 2025b), its potential in cross-modal reasoning remains underexplored. In this work, we extend it to understanding and transferring CoT reasoning capabilities across modalities.

Preliminary

Linear Artificial Tomography. Linear Artificial Tomography (LAT) is a representation reading technique for identifying internal representations of high-level concepts in deep neural networks (Zou et al. 2023). It serves as a tool for analyzing model behavior, which operates through a three-step process: (1) Designing Stimulus and Task, (2) Collecting Neural Activity, and (3) constructing a Linear Model.

First, to activate the model’s internal representation associated with a target concept or function f , LAT convert prompt $\{p_i\}_{i=1}^n$ into positive $\{p_i^+\}_{i=1}^n$ (elicits f) and negative $\{p_i^-\}_{i=1}^n$ (does not). Next, p_i^+ and p_i^- are fed into the model \mathcal{M} to extract hidden states $h_i^+(l)$ and $h_i^-(l)$ from layer l . In this paper, We extracts representations from final-token hidden states (Tang et al. 2025b). Finally, LAT constructs a linear model (Direction Represent) u . The mean of $\{u_i\}_{i=1}^n$ can be used as a transparent and interpretable method for analyzing or activating the concept.

Empirical Analysis

In this section, We first introduce the use of LAT in this work. We empirically analyze how VLM and LLM encode CoT reasoning apability using LAT.

Inducing and Capturing Internal Activations. To analyze the transferability of reasoning capabilities across modalities, we use LAT to observe the internal representations of LLMs and VLMs. Specifically, we first design two types of prompts: $\{q_i^+\}_{i=1}^n$ (i.e., "Let’s think step by step.") and $\{q_i^-\}_{i=1}^n$ (i.e., "Answer the question directly"). These prompts are separately fed into the LLM to generate the CoT responses $\{c_i\}_{i=1}^n$ and the non-CoT responses $\{d_i\}_{i=1}^n$. Given positive inputs $\{c_i\}_{i=1}^n$ and negative inputs $\{d_i\}_{i=1}^n$, we extract CoT representation sets $\{h_L(c_i, l)\}_{i=1}^n$ and $\{h_V(c_i, l)\}_{i=1}^n$, as well as vanilla representation sets $\{h_L(d_i, l)\}_{i=1}^n$ and $\{h_V(d_i, l)\}_{i=1}^n$, where h_L and h_V denote internal representations of the LLM and VLM. For our implementation, we use LLaMA3-8B (Meta 2024) to encode LLM representations and Qwen2-VL-7B-Instruct (Wang et al. 2024b) to encode VLM representations.

VLMs and LLMs have similar CoT reasoning encoding patterns. To better understand the properties of CoT representations and non-CoT representations within both LLMs and VLMs, we apply PCA (Jolliffe 2002) for dimensionality reduction and visualize the 2D representations. The visualization results are presented in Figure 1a. We observe that both VLMs and LLMs produce tightly clustered CoT representations across samples, which occupy distinct regions in the latent space compared to their non-CoT counterparts. These findings suggest that VLM and LLM have similar representational encoding schemes for CoT reasoning, despite

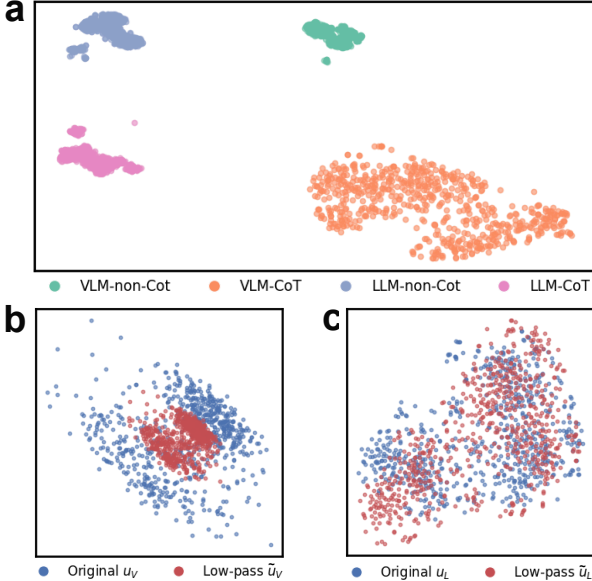


Figure 1: (a) Distribution of CoT and non-CoT representations in VLMs and LLMs. (b) Effect of low-pass filtering on VLM CoT direction representation. (c) Effect of low-pass filtering on LLM CoT direction representation.

their architectural differences. This consistency raises an question: *Can we leverage this shared encoding pattern to effectively transfer CoT reasoning capabilities from LLMs to VLMs?* However, we observe that the CoT representations of VLM cluster less tightly than LLM. The observed discrepancy is due to the heterogeneity between visual and textual modalities: when visual inputs are introduced and jointly trained with language, they induce representation drift in the high-dimensional latent space (Yang, Lu, and Yu 2024). This drift emerges from parameter updates during multimodal joint training and persists in the representations even when processing unimodal textual inputs (Park et al.). Consequently, this results in a gap between the CoT direction representations of LLMs and VLMs, which we will examine in detail in the following analysis.

Low-Frequency CoT direction representations of VLM encode CoT features and activate reasoning ability. We establish linear models to extract the CoT direction representation set $u_V(l)$ and $u_L(l)$ for VLM and LLM, respectively. Formally, these are defined as:

$$u_L(l) = \{h_L(c_i, l) - h_L(d_i, l)\}_{i=1}^n, \quad (1)$$

$$u_V(l) = \{h_V(c_i, l) - h_V(d_i, l)\}_{i=1}^n, \quad (2)$$

where $h(c_i, l)$ and $h(d_i, l)$ are hidden states at layer l corresponding to the CoT and non-CoT responses, computed by VLM (h_V) or LLM (h_L). To measure the dispersion of these representations, we compute the trace of their covariance matrix, where a larger trace indicates higher dispersion.

$$\text{Tr}(u(l)) = \frac{1}{n} \sum_{i=1}^n \|u_i - \bar{u}\|^2, \quad (3)$$

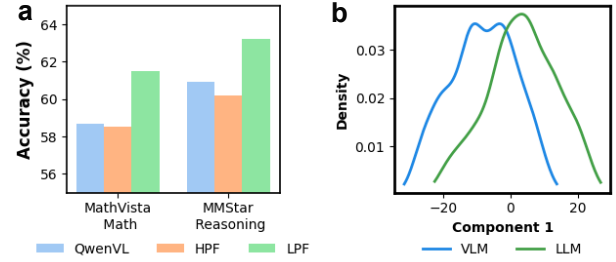


Figure 2: (a) Performance of Qwen2VL and its injected variants on MathVista-math and MMStar-reasoning. “HPF” injects high-frequency features. “LPF” injects low-frequency features. (b) The direction representation distribution for VLM and LLM after low-pass filtering (math domain).

where $\bar{u} = \frac{1}{n} \sum_{i=1}^n u_i$, and $\{u_i\}_{i=1}^n$ is drawn from either $u_L(l)$ or $u_V(l)$. We found that VLMs show significantly higher dispersion (1117.8) than LLMs (176.7). This divergence arises from the fundamental differences in architecture and training methods (Schrodi et al.). LLM capabilities are encoded through linearly separable structures in activation space (Burns et al. 2022), In contrast, VLMs have distinct optimization processes during multimodal pre-training. Consequently, components such as cross-modal attention, projection fusion, and alignment losses are incompatible with the LLM backbone. These inconsistencies introduce a more nonlinear and noisy activation space, ultimately causing shifts in internal representations of VLMs (Yang, Lu, and Yu 2024). To gain a deeper understanding of CoT direction representation shifts, we apply Fourier-domain low-pass filtering to the representations of VLMs, obtaining the low-frequency CoT direction representation $\tilde{u}_V(l)$:

$$\tilde{u}_V(l) = \text{Re} [\text{IFFT} (\mathbf{M}_k \odot \text{FFT}(u_V(l)))] , \quad (4)$$

where $\text{FFT}(\cdot)$ denotes the Fast Fourier Transform, $\text{IFFT}(\cdot)$ is its inverse operation, \odot represents Hadamard product and $\text{Re}[\cdot]$ extracts the real part to eliminate residual imaginary components. The low-pass mask $\mathbf{M}_k \in \{0, 1\}^d$, where d is the domain of $u_V(l)$, retains the first k frequency components and is defined as follows:

$$\mathbf{M}_k[i] = \begin{cases} 1, & \text{if } i < \frac{k}{2} \text{ or } i > d - \frac{k}{2}, \\ 0, & \text{otherwise.} \end{cases} \quad (5)$$

Figure 1b shows the distribution of the original $u_V(l)$ and filtered representations low-pass \tilde{u}_V . We can observe that filtered representations become significantly more concentrated, and the distribution shape stays stable. Quantitatively, trace drops from 1117.8 to 197.7 (close to LLM’s 176.7). For comparison, applying the same low-pass filtering to $u_L(l)$ just causes minimal change (Figure 1c). And we get the trace of low-pass \tilde{u}_L is 169.3, only slightly lower than the original value of 176.7. This indicates that filtering removes visual-specific noise while preserving LLM reasoning capability.

To verify if low-frequency filtering preserves CoT information, we average low and high-frequency VLM direction representations and inject them into the VLM. We conduct experiments on the MathVista and MMStar datasets (detailed in the Experiments section). The results are shown

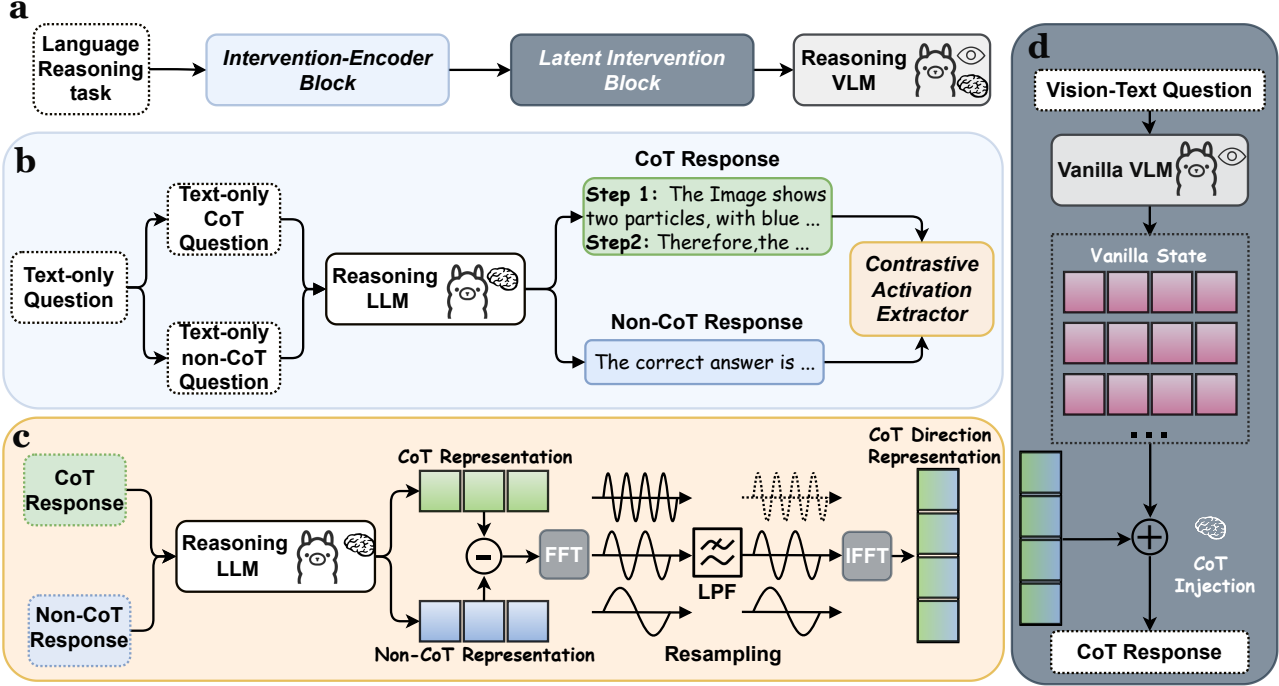


Figure 3: (a) The overview of Latent Intervention for LLM-to-VLM CoT Transfertion (L2V-CoT). (b) The block of Intervention-Encoder. (c) Low-pass LLM CoT direction representation extraction process. (d) The block of Latent Intervention.

in Figure 2. We observe that only low-frequency direction representation enhances the reasoning ability of VLM. This further shows that low-frequency CoT direction representations in VLMs carry CoT information and can be used to enhance the reasoning ability of model.

Distribution of Low-Frequency CoT direction representations in VLM and LLM exhibit substantial overlap. Due to the scarcity of multimodal reasoning data, the reasoning ability of VLMs falls far behind that of LLMs. Although low-frequency CoT directions can enhance the VLM reasoning abilities, they still limited by the capacity of the VLM itself. *To overcome this bottleneck, we investigate transferring the superior reasoning capabilities of LLMs to VLMs via latent intervention.* To support this, we analyze the alignment between low-frequency CoT direction representations of VLMs and LLMs. As shown in Figure 2b, their PCA-projected 1D distributions exhibit substantial overlap, indicating a shared latent structure. This indicates the potential for effective knowledge transfer without significant domain mismatch. Consequently, this empirical observation provides strong evidence supporting the feasibility of transferring reasoning capabilities across modalities and disparate model architectures through latent interventions.

CoT Reasoning Capability transfer via Latent Intervention

As previously discussed, LLM and VLM have similar low-pass CoT direction representations. This suggests that the CoT capabilities of LLMs can be transferred to VLMs. We

extract CoT direction representations from LLM and inject them to VLMs. However, due to representation dimension mismatch between different architectures, we apply low-pass filtering and resampling in the latent space to align dimension while minimizing the loss of CoT ability. Figure 3 shows the framework. In this section, we first describe the extraction of low-pass CoT pattern representations and then introduce how these direction representations are used to perform latent intervention on vanilla VLMs.

Extraction of low-pass CoT pattern representations

As shown in Figure 3b and formalized in Eq. 1, we first collect positive inputs $\{c_i\}_{i=1}^n$ and negative inputs $\{d_i\}_{i=1}^n$ from an LLM with predefined questions $\{q_i\}_{i=1}^n$. These pairs are yield CoT direction representations $\{u_i(l_L)\}_{i=1}^n$ in the LLM. For unbiased transfer the general CoT reasoning capability of LLM, we compute the mean of $\{u_i(l_L)\}_{i=1}^n$ to get the CoT pattern representation $v(l_L)$:

$$v(l_L) = \frac{1}{n} \sum_{i=1}^n (h_L(c_i, l_L) - h_L(d_i, l_L)), \quad (6)$$

where l_L is the index of the layer from which the representation is extracted in LLM. Due to potentially different LLM backbones in the LLM and VLM, we must match their representation dimension. As shown earlier, LPF can preserve CoT information in the direction representations. Therefore, we apply LMN method (Gerlach et al. 2024) to resample $\{u_i(l_L)\}_{i=1}^n$ in the frequency domain. This helps reduce the loss of CoT information during dimension alignment. This

Model	Method	MathVista			MathVerse Benchmarks					MMStar			DM	MV	Avg.	
		All	General	Math	Overall	T-D	T-L	V-I	V-D	V-O	All	Percep.	Reason.			
LLAVA	Non-CoT response	35.2	46.7	25.3	20.9	24.0	20.9	21.5	20.0	18.2	43.4	52.8	38.7	22.9	12.8	27.0
	Few-Shot CoT	33.7	45.8	23.4	19.3	22.8	19.3	19.7	18.4	16.5	40.4	49.5	35.9	21.1	11.5	25.2
	MathNeuro	35.8	46.6	26.6	21.5	24.6	21.5	21.7	20.8	18.9	44.1	51.3	40.5	23.0	13.4	27.6
	Modal Merging	36.4	45.3	28.8	21.9	26.8	22.4	22.9	20.8	16.6	43.6	51.3	39.8	23.5	13.4	27.8
	RoT	36.8	47.3	27.9	22.9	25.8	23.3	23.1	22.0	20.5	45.6	53.1	41.9	24.8	14.8	29.0
	Finetuned CoT	39.9	49.1	32.0	24.1	27.6	24.8	24.0	22.6	21.6	47.0	54.4	43.3	25.8	15.6	30.5
	L2V-COT (ours)	41.8	51.0	34.0	25.5	25.9	25.0	23.2	23.7	48.1	55.6	44.3	26.9	16.2	31.6	
InternVL	Non-CoT response	59.3	62.8	56.3	29.9	30.2	33.4	30.8	32.1	23.0	59.5	58.0	60.3	30.5	19.6	39.8
	Few-Shot CoT	57.4	61.2	54.1	27.9	28.6	31.1	28.4	30.2	21.1	57.8	56.3	58.5	28.9	18.2	38.0
	MathNeuro	59.9	63.1	57.1	30.2	31.0	34.1	31.3	31.0	23.8	59.9	57.5	61.1	31.6	21.0	40.5
	Modal Merging	60.4	63.4	57.8	30.9	30.3	34.6	32.5	33.2	24.1	59.3	58.5	59.7	31.9	21.1	40.7
	RoT	60.7	63.3	58.5	31.1	32.2	34.5	32.0	32.5	24.3	60.9	58.4	62.1	32.3	21.3	41.3
	Finetuned CoT	61.2	63.5	59.3	32.6	35.4	35.3	33.1	33.6	25.5	61.6	59.0	62.9	33.2	21.9	42.1
	L2V-COT (ours)	61.6	63.5	60.0	33.3	37.2	35.4	33.9	34.0	26.1	62.0	59.1	63.5	33.7	22.3	42.6
QwenVL	Non-CoT response	60.5	62.6	58.7	26.9	28.6	27.4	27.8	29.4	21.1	63.1	67.4	60.9	33.8	19.1	40.7
	Few-Shot CoT	58.4	61.3	56.0	25.3	26.5	26.2	26.4	27.7	19.5	60.2	64.1	58.2	31.9	17.6	38.7
	MathNeuro	61.8	63.3	60.5	28.6	30.1	29.8	29.6	30.7	23.0	62.6	64.0	61.9	32.8	21.0	41.4
	Modal Merging	61.5	62.3	60.8	29.9	32.6	30.3	29.1	31.9	25.7	63.0	66.1	61.5	34.1	20.3	41.8
	RoT	62.9	65.0	61.2	29.7	31.4	30.2	30.0	31.1	25.8	64.4	67.1	63.0	35.1	21.5	42.7
	Finetuned CoT	63.7	65.4	62.3	32.8	35.1	33.8	32.4	34.4	28.2	65.0	67.9	63.5	35.3	22.1	43.8
	L2V-COT (ours)	64.2	65.9	62.8	35.5	37.9	34.9	34.5	36.7	33.3	65.5	68.2	64.1	35.9	22.6	44.7
Idefics	Non-CoT response	48.4	51.7	45.6	19.8	22.87	21.85	20.97	21.2	12.1	49.2	54.0	46.8	25.9	16.5	32.0
	Few-Shot CoT	46.3	50.2	43.0	18.1	21.2	20.0	19.4	19.6	10.3	46.8	51.3	44.5	24.3	14.9	30.1
	MathNeuro	49.1	52.4	46.3	19.8	23.4	22.1	20.1	22.0	11.5	49.4	54.1	47.1	26.2	15.9	32.1
	Modal Merging	49.3	52.3	46.8	21.0	24.5	23.1	21.5	22.6	13.1	49.7	53.2	47.9	26.3	16.1	32.5
	RoT	49.6	52.8	46.9	20.7	24.1	22.6	21.3	22.5	12.8	49.9	54.5	47.6	26.4	17.5	32.8
	Finetuned CoT	50.5	53.4	48.1	22.3	25.4	24.2	22.9	24.6	14.4	51.4	55.4	49.4	28.1	18.6	34.2
	L2V-COT (ours)	51.8	54.3	49.7	23.5	26.3	25.5	24.6	25.9	15.3	52.3	56.3	50.3	29.3	19.2	35.2

Table 1: Performance comparison of different methods across the MathVista (All, General, and Math-related categories), MathVerse, MMStar (All, Perception, and Reasoning categories), DynaMath (DM), and MathVision (MV) benchmarks. The best result for each task is highlighted in bold. All results are the mean values of five runs using different random seeds.

processing is illustrated in Figure 3c. FFT and IFFT are both linear transformations. For computational efficiency, we directly apply the low-pass filter to the aggregated CoT pattern representation $v(l_L)$, obtaining the low-pass CoT pattern representation $v_{LPF}(l_L)$:

$$v_{LPF}(l_L) = \text{Re} [\text{IFFT} (\text{LMN} (\mathbf{M}_k \odot \text{FFT}(v(l_L))))], \quad (7)$$

where LMN is resampling method in frequency domain. Since low-pass filtering reduces the energy, we normalize the resulting vector to preserve its directional information and enhance the effectiveness of injection:

$$\hat{v}_{LPF}(l_L) = \frac{\|v(l_L)\|_2}{\|v_{LPF}(l_L)\|_2} v_{LPF}(l_L). \quad (8)$$

Latent Intervention

As shown in Figure 1d, we inject the low-pass CoT pattern $v_{LPF}(l_L)$ into the hidden representation $h_V(l_V)$ of the Vanilla VLM at layer l_V during inference, thereby transferring the reasoning patterns from the LLM to the VLM. Here, $h_V(l_V)$ denotes the internal neural representation of the VLM activated by the vision-text input during the inference process. To preserve the original capacity of VLM, we follow Tang et al. (2025b) to normalize the updated neural activations after injecting the CoT capability, thereby reducing interference with the original representation space:

$$\hat{h}_V(l_V) = h_V(l_V) + \alpha \cdot \hat{v}_{LPF}(l_L), \quad (9)$$

$$\hat{h}_V(l_V) = \frac{\|h_V(l_V)\|_2}{\|\hat{h}_V(l_V)\|_2} \hat{h}_V(l_V), \quad (10)$$

where $\alpha \in \mathbb{R}^+$ denotes a positive coefficient that modulates the strength of the injection.

Experiments

In this section, we first describe the experimental setup, then analyze the main experimental results, and finally conduct further analysis.

Experimental Setup

Building CoT Reasoning Samples. To transfer the CoT reasoning capability of LLMs, we use the open-source dataset STILL-2 (Min et al. 2024) to extract both CoT responses and non-CoT responses. STILL distills high-quality CoT answers and direct answers from existing large-scale reasoning models (Guo et al. 2025). Following Tang et al. (2025b), we randomly sample 100 examples from each of four domains: math, physics, chemistry, and biology to obtain generalizable CoT pattern representations.

VLMs and LLMs. We apply L2V-CoT to a variety of VLM architectures to evaluate the generalizability. Specifically, we conduct experiments on LLaVA-Next-LLaMA3-8B (Liu et al. 2024), Idefics2-8B (Laurençon et al. 2024), Qwen2-VL-7B-Instruct (Wang et al. 2024b), and InternVL2-8B (Chen et al. 2024c) (abbreviated as LLaVA, Idefics, QwenVL, and InternVL). For representation transfer, we use DeepSeek-R1-Distill-Qwen-32B (Guo et al. 2025; Wang et al. 2024b), a model with strong reasoning ability. During injection, we align and inject the middle layers of LLM and VLM. Details are provided in Appendix E.

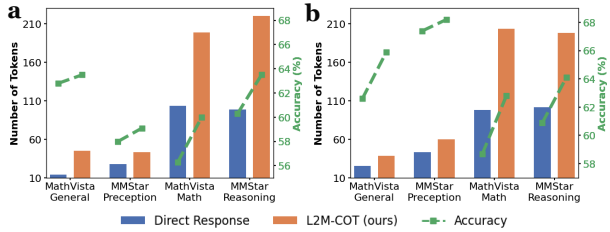


Figure 4: Effect on Response Length and Accuracy. (a) InternVL2-8B. (b) Qwen2-VL-7B-Instruct.

Datasets. To assess the effectiveness of L2V-CoT, we evaluate it on five benchmark: MathVista (Lu et al. 2023), MathVerse (Zhang et al. 2024), MathVision (Wang et al. 2024a), Dynamath (Zou et al. 2024), and MMStar (Chen et al. 2024a). MathVerse, MathVision, and DynaMath cover algebra, geometry, and calculus, suitable task, making them well suited for evaluating the reasoning capability of model. MathVista and MMStar contain more diverse vision tasks, enabling a more comprehensive assessment of models’ multifaceted abilities. Detailed can be seen in Appendix F.

Baselines. To demonstrate the effectiveness of our approach, we compare it with several representative baselines: non-CoT response, CoT demonstration method (Few-shot CoT), neuron activation method (MathNeuro) (Christ et al. 2024), representation engineering approach (RoT) (Hu et al. 2024), supervised fine-tuning (Finetuned CoT) (Du et al. 2025), and Model Merging (Chen et al. 2025).

L2V-CoT Substantially Improves the Reasoning Capabilities of VLMs Through Controlled Slow Thinking Injection

The experimental results are shown in Table 1. Few-shot CoT performs worse than non-CoT response. This is mainly because the reasoning process varies across different questions. The reasoning paths in the examples are often not generalizable and may even mislead the model’s reasoning. Unlike such explicit prompting methods, MathNeuro improves VLMs by activating reasoning-related neurons but overlooks their coordination. Modal Merging addresses this by combining a VLM and an LLM that share the same backbone. This method transfers the reasoning ability from the LLM and brings moderate improvements. However, it performs parameter-level fusion and lacks alignment between the transferred LLM and the visual modality. In contrast, RoT achieves more significant improvements. It introduces controllable reasoning activation by contrasting CoT and non-CoT prompts within the VLM’s latent space. Nevertheless, RoT remains constrained by the inherent reasoning limitations of the VLM and does not facilitate the transfer of the more powerful reasoning capabilities from LLMs to VLMs.

Compared to these train-free baselines, our method achieves significantly better performance. Notably, it also outperforms models that are supervised-finetuned on datasets used to build CoT pattern representations. This improvement comes mainly from CoT pattern representations from LLM. We apply latent intervention to switch the la-

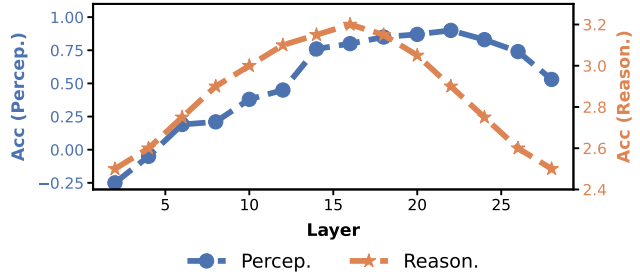


Figure 5: Qwen2-VL-7B-Instruct accuracy gain on MMStar with L2V-CoT injection at different layers. Y-axis indicates accuracy change over non-CoT responses.

tent space of VLM into slow-thinking mode. In this mode, the VLM is able to decompose a problem into a series of intermediate reasoning steps, which enhances its reasoning ability. A key indicator of this mode is the increased answer length. To verify that L2V-CoT transfers the slow-thinking pattern from LLMs to VLMs, we visualize the changes in answer length and accuracy on MathVista and MMStar in Figure 5. The results show that our method transfers the reasoning capability of LLMs into VLMs through latent intervention. We also observe that for tasks requiring reasoning, such as MathVista-Math and MMStar-Reasoning, the model produces significantly longer outputs and achieves greater performance improvements.

Detailed Analysis

Layer-wise Representation Injection Universally Boosts Reasoning in Vision-Language Models. We analyze layer-wise injection effects using Qwen2-VL-7B-Instruct, as shown in Figure 5. The results show that as the injection layer increases, the performance gain first rises and then declines. This is because lower layers encode perception features, while middle and upper layers handle reasoning (Chen et al. 2025). Injecting into lower layers disturbs perception. As a result, for perception tasks, injecting representations at shallow layers can even hurt performance, and the optimal injection layer tends to be deeper. In contrast, reasoning tasks benefit from early-layer injection. Additionally, when injecting into higher layers, the remaining layers are not sufficient to process the injected representations, which also leads to performance degradation. Notably, injection at any layer consistently enhances VLM reasoning.

L2V-CoT Enhances Explicit Models through Complementary Reasoning Integration. Explicit methods guide the reasoning process by a predefined search structure (e.g., Monte Carlo Tree Search) and a reward model. In contrast, L2V-CoT changes VLM reasoning mode via latent intervention. These are orthogonal and combinable. We combine our method with the explicit method Mulberry (Yao et al. 2024), and present the results in Figure 6. The results show that our method leads to further performance improvements.

Injecting Representations with Moderate Strength Significantly Boosts Reasoning Performance. Injection Strength is key in our method. We study its impact on the per-

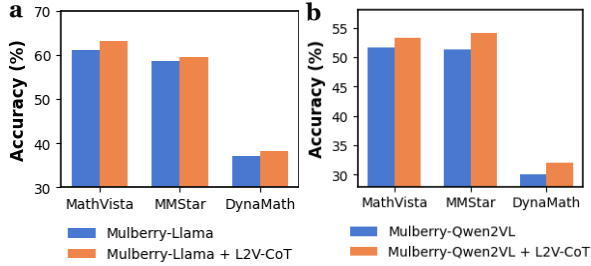


Figure 6: Performance of the explicit method *Mulberry* combined with L2V-CoT. (a) Llama-11B. (b) Qwen2VL-2B.

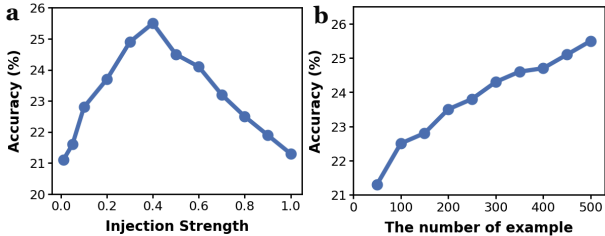


Figure 7: Effect of injection strength and CoT example number on LLaVA's MathVerse performance (LLaVA-Next-LLaMA3-8B performance on MathVerse). (a) Injection strength. (b) Number of CoT examples.

formance of L2V-CoT. The results are shown in Figure 7a. When the injection strength is low, the model cannot effectively absorb the reasoning ability from the LLM. As a result, the performance rises with increasing strength. However, when the injection strength becomes too high, the injected representation may disrupt the original semantic information. This can lead to a drop in performance. Overall, representation injection consistently improves model performance. The best performance gain is achieved when the injection strength is set to a moderate level.

Performance Improves with More CoT Examples. L2V-CoT uses LLM CoT examples extract representation. We investigate how example count affects performance. The results are shown in Figure 7b. We can observe that performance improves with more examples. This is because few examples yield CoT patterns with excessive domain bias. With more examples, L2V-CoT can extract more general and robust CoT pattern representations. This leads to better transfer of the LLM's reasoning ability.

L2V-CoT Generalizes Well Across Models of Varying Sizes. We test our method on InternVL2-series VLMs using MathVista and MMStar. The results are shown in Figure 8. We observe that L2V-CoT consistently achieves strong performance across models of different sizes. This further demonstrates the effectiveness of our approach.

LPF Method and LLM Representations Effectively Transfer LLM Reasoning Ability. To demonstrate the effectiveness of the LPF method and LLM representations,

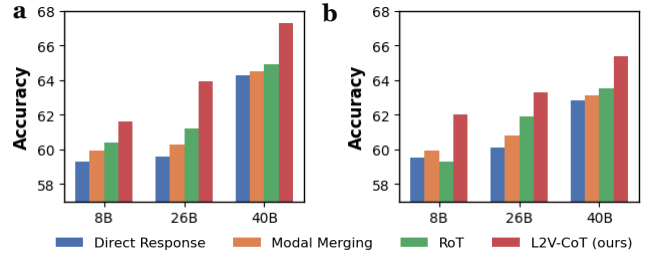


Figure 8: Performance of InternVL2-series VLMs on MathVista and MMStar benchmarks. (a) MathVista. (b) MMStar.

Model	Method	MathVista	MathVerse	DynaMath
LLAVA	Direct Response	35.2	20.9	22.9
	L2V-COT	41.8	25.5	26.9
InternVL	w interpolation	31.1	16.3	19.4
	w VLM	36.3	22.5	23.2
QwenVL	Direct Response	59.3	29.9	30.5
	L2V-COT	61.6	33.3	33.7
	w interpolation	53.6	21.3	19.1
	w VLM	60.1	30.9	31.3

Table 2: Ablation study of L2V-CoT. "w interpolation" denotes replacing the LMN method with an interpolation-based method in L2V-COT. "w VLM" uses VLM's low-pass direction representation to activate its reasoning.

we conduct an ablation study on L2V-CoT. Specifically, we test two variants: "w interpolation" replaces LPF with interpolation and "w VLM" uses low-pass direction representation for injection. The results are shown in Table 2. We find that interpolation leads to performance degradation. This is because interpolation causes significant loss of CoT information. As a result, it not only fails to improve the model's reasoning ability, but also weakens its original performance. Injecting VLM representations performs worse than injecting LLM representations. This is mainly because LLM representations help transfer the reasoning ability of the LLM, which is much stronger than that of the VLM.

Conclusion

In this paper, we empirically analyze CoT reasoning representations across modalities and architectures using LAT. Our analysis reveals that low-pass CoT direction representations effectively activate reasoning abilities in VLMs and exhibit similar distributions between VLMs and LLMs. Motivated by this insight, we propose L2V-CoT, a training-free method to transfer CoT reasoning capabilities from LLMs to VLMs. Specifically, we extract CoT direction representations from LLMs, performs frequency-domain resampling to align with VLM representation dimension, and injects the resampled representation into VLMs. Extensive experiments demonstrate that L2V-CoT significantly enhances VLM reasoning performance, achieving an average improvement of 3.7% and up to 8.6% across various benchmarks.

Acknowledgments

The work is supported by the National Natural Science Foundation of China (No. 92270118 and No. 62276269) and the Beijing Natural Science Foundation (No. 1232009).

References

Burns, C.; Ye, H.; Klein, D.; and Steinhardt, J. 2022. Discovering latent knowledge in language models without supervision. *arXiv preprint arXiv:2212.03827*.

Chen, L.; Li, J.; Dong, X.; Zhang, P.; Zang, Y.; Chen, Z.; Duan, H.; Wang, J.; Qiao, Y.; Lin, D.; et al. 2024a. Are we on the right way for evaluating large vision-language models? *Advances in Neural Information Processing Systems*, 37: 27056–27087.

Chen, Q.; Qin, L.; Zhang, J.; Chen, Z.; Xu, X.; and Che, W. 2024b. M³CoT: A Novel Benchmark for Multi-Domain Multi-step Multi-modal Chain-of-Thought. In Ku, L.-W.; Martins, A.; and Srikumar, V., eds., *Proceedings of the 62nd Annual Meeting of the Association for Computational Linguistics (Volume 1: Long Papers)*, 8199–8221. Bangkok, Thailand: Association for Computational Linguistics.

Chen, S.; Zhang, J.; Zhu, T.; Liu, W.; Gao, S.; Xiong, M.; Li, M.; and He, J. 2025. Bring reason to vision: Understanding perception and reasoning through model merging. *arXiv preprint arXiv:2505.05464*.

Chen, Z.; Wu, J.; Wang, W.; Su, W.; Chen, G.; Xing, S.; Zhong, M.; Zhang, Q.; Zhu, X.; Lu, L.; et al. 2024c. Internvl: Scaling up vision foundation models and aligning for generic visual-linguistic tasks. In *Proceedings of the IEEE/CVF conference on computer vision and pattern recognition*, 24185–24198.

Cheng, Z.; Chen, Q.; Zhang, J.; Fei, H.; Feng, X.; Che, W.; Li, M.; and Qin, L. 2025. Comt: A novel benchmark for chain of multi-modal thought on large vision-language models. In *Proceedings of the AAAI Conference on Artificial Intelligence*, volume 39, 23678–23686.

Christ, B. R.; Gottesman, Z.; Kropko, J.; and Hartvigsen, T. 2024. Math Neurosurgery: Isolating Language Models’ Math Reasoning Abilities Using Only Forward Passes. *arXiv preprint arXiv:2410.16930*.

Du, Y.; Liu, Z.; Li, Y.; Zhao, W. X.; Huo, Y.; Wang, B.; Chen, W.; Liu, Z.; Wang, Z.; and Wen, J.-R. 2025. Virgo: A preliminary exploration on reproducing o1-like mllm. *arXiv preprint arXiv:2501.01904*.

Gerlach, L.; Gu, W.; Nayak, N.; Qian, X.; and Viren, B. 2024. Waveform resampling with LMN method. *Journal of Instrumentation*, 19(10): P10029.

Guo, D.; Yang, D.; Zhang, H.; Song, J.; Zhang, R.; Xu, R.; Zhu, Q.; Ma, S.; Wang, P.; Bi, X.; et al. 2025. Deepseek-r1: Incentivizing reasoning capability in llms via reinforcement learning. *arXiv preprint arXiv:2501.12948*.

Hartsock, I.; and Rasool, G. 2024. Vision-language models for medical report generation and visual question answering: A review. *Frontiers in artificial intelligence*, 7: 1430984.

Hu, L.; Liu, L.; Yang, S.; Chen, X.; Tan, Z.; Ali, M. A.; Li, M.; and Wang, D. 2024. Understanding reasoning in chain-of-thought from the hopfieldian view. *arXiv preprint arXiv:2410.03595*.

Jolliffe, I. T. 2002. Springer series in statistics. *Principal component analysis*, 29: 912.

Kelkar, S.; Grigsby, L.; and Langsner, J. 2007. An extension of Parseval’s theorem and its use in calculating transient energy in the frequency domain. *IEEE Transactions on Industrial Electronics*, (1): 42–45.

Kim, Y.-J.; Kim, M.-J.; An, K.; Ahn, J.; Kim, J.; Heo, Y.-J.; Chang, D.-S.; and Kim, E.-S. 2024. Structure-aware multimodal sequential learning for visual dialog. In *Proceedings of the AAAI Conference on Artificial Intelligence*, volume 38, 13193–13201.

Laurençon, H.; Tronchon, L.; Cord, M.; and Sanh, V. 2024. What matters when building vision-language models? *Advances in Neural Information Processing Systems*, 37: 87874–87907.

Li, K.; Patel, O.; Viégas, F.; Pfister, H.; and Wattenberg, M. 2023. Inference-time intervention: Eliciting truthful answers from a language model. *Advances in Neural Information Processing Systems*, 36: 41451–41530.

Li, Y.; Chen, Z.; Wu, Z.; Zhou, K.; Luo, R.; Zhang, C.; He, Z.; Zhan, Y.; Zhao, W. X.; and Qiu, M. 2025a. Unleashing Perception-Time Scaling to Multimodal Reasoning Models. *arXiv preprint arXiv:2510.08964*.

Li, Y.; Guo, H.; Zhou, K.; Zhao, W. X.; and Wen, J.-R. 2024. Images are Achilles’ heel of alignment: Exploiting visual vulnerabilities for jailbreaking multimodal large language models. In *European Conference on Computer Vision*, 174–189. Springer.

Li, Y.; Zhou, K.; Zhao, W. X.; Fang, L.; and Wen, J.-R. 2025b. Analyzing and Mitigating Object Hallucination: A Training Bias Perspective. *arXiv preprint arXiv:2508.04567*.

Liu, H.; Li, C.; Li, Y.; Li, B.; Zhang, Y.; Shen, S.; and Lee, Y. J. 2024. Llava-next: Improved reasoning, ocr, and world knowledge, January 2024. URL <https://llava-vl.github.io/blog/2024-01-30-llava-next>, 1(8).

Liu, Z.; Zhou, K.; Zhao, W. X.; Gao, D.; Li, Y.; and Wen, J.-R. 2025. Do we Really Need Visual Instructions? Towards Visual Instruction-Free Fine-tuning for Large Vision-Language Models. *arXiv preprint arXiv:2502.11427*.

Lu, P.; Bansal, H.; Xia, T.; Liu, J.; Li, C.; Hajishirzi, H.; Cheng, H.; Chang, K.-W.; Galley, M.; and Gao, J. 2023. Mathvista: Evaluating mathematical reasoning of foundation models in visual contexts. *arXiv preprint arXiv:2310.02255*.

Luo, R.; Zheng, Z.; Wang, Y.; Ni, X.; Lin, Z.; Jiang, S.; Yu, Y.; Shi, C.; Chu, R.; Zeng, J.; et al. 2025. Ursu: Understanding and verifying chain-of-thought reasoning in multimodal mathematics. *arXiv preprint arXiv:2501.04686*.

Meta, A. 2024. Introducing meta llama 3: The most capable openly available llm to date. *Meta AI*, 2(5): 6.

Min, Y.; Chen, Z.; Jiang, J.; Chen, J.; Deng, J.; Hu, Y.; Tang, Y.; Wang, J.; Cheng, X.; Song, H.; et al. 2024.

Imitate, explore, and self-improve: A reproduction report on slow-thinking reasoning systems. *arXiv preprint arXiv:2412.09413*.

OpenAI. 2024. Learning to Reason with Large Language Models. OpenAI Blog and arXiv preprint. <https://openai.com/index/learning-to-reason-with-langs/> (accessed 2024-09-29).

Park, S.; Panigrahi, A.; Cheng, Y.; Yu, D.; Goyal, A.; and Arora, S. ???? Generalizing from SIMPLE to HARD Visual Reasoning: Can We Mitigate Modality Imbalance in VLMs? In *Forty-second International Conference on Machine Learning*.

Schrodi, S.; Hoffmann, D. T.; Argus, M.; Fischer, V.; and Brox, T. ???? Two Effects, One Trigger: On the Modality Gap, Object Bias, and Information Imbalance in Contrastive Vision-Language Models. In *The Thirteenth International Conference on Learning Representations*.

Tang, X.; Lv, Z.; Cheng, X.; Li, J.; Zhao, W. X.; Wen, Z.; Zhang, Z.; and Zhou, J. 2025a. Enhancing Cross-task Transfer of Large Language Models via Activation Steering. *arXiv preprint arXiv:2507.13236*.

Tang, X.; Wang, X.; Lv, Z.; Min, Y.; Zhao, W. X.; Hu, B.; Liu, Z.; and Zhang, Z. 2025b. Unlocking General Long Chain-of-Thought Reasoning Capabilities of Large Language Models via Representation Engineering. *CoRR*.

Thawakar, O.; Dissanayake, D.; More, K.; Thawakar, R.; Heakl, A.; Ahsan, N.; Li, Y.; Zumri, M.; Lahoud, J.; Anwer, R. M.; et al. 2025. Llamav-o1: Rethinking step-by-step visual reasoning in llms. *arXiv preprint arXiv:2501.06186*.

Tigges, C.; Hollingsworth, O. J.; Geiger, A.; and Nanda, N. 2024. Language Models Linearly Represent Sentiment. In Belinkov, Y.; Kim, N.; Jumelet, J.; Mohebbi, H.; Mueller, A.; and Chen, H., eds., *Proceedings of the 7th BlackboxNLP Workshop: Analyzing and Interpreting Neural Networks for NLP*, 58–87. Miami, Florida, US: Association for Computational Linguistics.

Wang, K.; Pan, J.; Shi, W.; Lu, Z.; Ren, H.; Zhou, A.; Zhan, M.; and Li, H. 2024a. Measuring multimodal mathematical reasoning with math-vision dataset. *Advances in Neural Information Processing Systems*, 37: 95095–95169.

Wang, P.; Bai, S.; Tan, S.; Wang, S.; Fan, Z.; Bai, J.; Chen, K.; Liu, X.; Wang, J.; Ge, W.; et al. 2024b. Qwen2-vl: Enhancing vision-language model’s perception of the world at any resolution. *arXiv preprint arXiv:2409.12191*.

Wang, Y.; Ren, R.; Wang, Y.; Liu, J.; Zhao, W. X.; Wu, H.; and Wang, H. 2025a. BEE-RAG: Balanced Entropy Engineering for Retrieval-Augmented Generation. *arXiv preprint arXiv:2508.05100*.

Wang, Y.; Ren, R.; Wang, Y.; Zhao, W. X.; Liu, J.; Wu, H.; and Wang, H. 2025b. Unveiling Knowledge Utilization Mechanisms in LLM-based Retrieval-Augmented Generation. In *Proceedings of the 48th International ACM SIGIR Conference on Research and Development in Information Retrieval*, 1262–1271.

Wu, J.; Feng, M.; Zhang, S.; Jin, R.; Che, F.; Wen, Z.; and Tao, J. 2025. Boosting multimodal reasoning with mcts-automated structured thinking. *arXiv e-prints*, arXiv–2502.

Xia, Y.; Wang, R.; Liu, X.; Li, M.; Yu, T.; Chen, X.; McAuley, J.; and Li, S. 2024. Beyond chain-of-thought: A survey of chain-of-x paradigms for llms. *arXiv preprint arXiv:2404.15676*.

Yang, X.; Lu, J.; and Yu, E. 2024. Adapting multi-modal large language model to concept drift from pre-training onwards. *arXiv preprint arXiv:2405.13459*.

Yao, H.; Huang, J.; Wu, W.; Zhang, J.; Wang, Y.; Liu, S.; Wang, Y.; Song, Y.; Feng, H.; Shen, L.; et al. 2024. Mulberry: Empowering mllm with o1-like reasoning and reflection via collective monte carlo tree search. *arXiv preprint arXiv:2412.18319*.

Zhan, Y.-L.; Lu, Z.-Y.; Sun, H.; and Gao, Z.-F. 2024. Over-parameterized student model via tensor decomposition boosted knowledge distillation. *Advances in Neural Information Processing Systems*, 37: 69445–69470.

Zhang, R.; Jiang, D.; Zhang, Y.; Lin, H.; Guo, Z.; Qiu, P.; Zhou, A.; Lu, P.; Chang, K.-W.; Qiao, Y.; et al. 2024. Mathverse: Does your multi-modal llm truly see the diagrams in visual math problems? In *European Conference on Computer Vision*, 169–186. Springer.

Zhang, Y.; Wang, X.; Wu, L.; and Wang, J. 2025. Enhancing chain of thought prompting in large language models via reasoning patterns. In *Proceedings of the AAAI Conference on Artificial Intelligence*, volume 39, 25985–25993.

Zhang, Z.; Zhang, A.; Li, M.; Zhao, H.; Karypis, G.; and Smola, A. 2023. Multimodal chain-of-thought reasoning in language models. *arXiv preprint arXiv:2302.00923*.

Zou, A.; Phan, L.; Chen, S.; Campbell, J.; Guo, P.; Ren, R.; Pan, A.; Yin, X.; Mazeika, M.; Dombrowski, A.-K.; et al. 2023. Representation engineering: A top-down approach to ai transparency. *arXiv preprint arXiv:2310.01405*.

Zou, C.; Guo, X.; Yang, R.; Zhang, J.; Hu, B.; and Zhang, H. 2024. Dynamath: A dynamic visual benchmark for evaluating mathematical reasoning robustness of vision language models. *arXiv preprint arXiv:2411.00836*.

APPENDIX

A Detailed Description of Baselines

Tang et al. (2025b) selected representative baselines to demonstrate the effectiveness of the proposed GLoRE method when showing that activation engineering can unlock the long CoT abilities of LLMs. We follow GLoRE and use baselines: Non-CoT response, Few-shot CoT, Math-Neuro (Christ et al. 2024), and RoT (Hu et al. 2024). In addition, we include several VLM-specific methods that aim to transfer reasoning from LLMs as baselines: Finetuned CoT (Du et al. 2025) and Model Merging (Chen et al. 2025). In this section, we describe each baseline in detail.

Non-CoT response: This method uses a vanilla VLM prompted with a CoT-style instruction (e.g., "Answer the question step by step and put the final answer in $\boxed{\text{}}$ "). The VLM responds to the question and places the final answer inside $\boxed{\text{}}$.

Few-shot CoT: This method provides the VLM with CoT answers generated by an LLM as examples. The model learns to imitate the reasoning ability of LLM through instruction-based prompting.

MathNeuro (Christ et al. 2024): By analyzing the forward pass weights and activations, MathNeuro pinpoints parameters crucial for reasoning and selectively refines them via pruning and scaling.

RoT (Hu et al. 2024): This method also uses representation injection. However, unlike our approach which injects representations from CoT answers, RoT extracts representations from CoT prompts and injects them into the VLM.

Finetuned CoT (Du et al. 2025): This method directly fine-tunes the VLM using the same data we use to obtain CoT direction representations. The goal is to teach the model the CoT reasoning pattern through supervised learning.

Model Merging (Chen et al. 2025): This method merges a VLM and an LLM that share the same backbone. It transfers the reasoning ability from the LLM to the VLM to enhance the model's reasoning performance.

B Spectral Similarity Between VLMs and LLMs

In signal processing, differences between signals are often evaluated by comparing their energy across frequency bands (Kelkar, Grigsby, and Langsner 2007). We compute the relative error of CoT direction representations between LLM and VLM in each frequency band. As shown in Figure S.1, the error in the low-frequency band (Band 1) is much smaller than in the high-frequency bands. This further supports our empirical finding: the low-pass filtered direction representations of VLM are close to those of LLM.

C Stronger LLMs Enable Stronger Performance Transfer.

We further investigate how the capability of the LLM influences the transferred performance of the VLM. Specifically, we use different sizes of DeepSeek-R1-Distill-Qwen to extract CoT pattern representations. As shown in Table S.1,

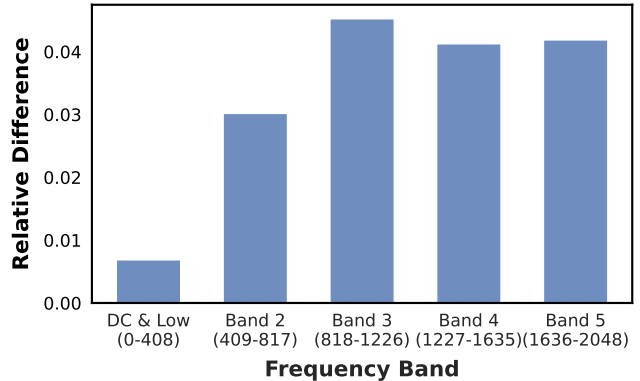


Figure S.1: Relative energy difference across frequency bands between the CoT direction representations of the VLM (Qwen2-VL-7B-Instruct) and the LLM (LLaMA3-8B). "DC&Low" denotes the low-frequency band, while the others correspond to mid- and high-frequency bands.

Model	Method	MathVista	MathVerse	DynaMath
LLAVA	Direct Response	35.2	20.9	22.9
	L2V-COT-7B	38.6	23.7	24.2
	L2V-COT-14B	38.9	24.4	24.9
	L2V-COT-32B	41.8	25.5	26.9
InternVL	Direct Response	59.3	29.9	30.5
	L2V-COT-7B	60.9	31.1	31.6
	L2V-COT-14B	61.0	31.9	32.6
	L2V-COT-32B	61.6	33.3	33.7
QwenVL	Direct Response	60.5	26.9	33.8
	L2V-COT-7B	61.6	29.4	34.2
	L2V-COT-14B	62.3	31.8	34.5
	L2V-COT-32B	64.2	35.5	35.9

Table S.1: Performance of L2V-CoT with different LLM representation. 7B, 14B, and 32B refer to the model sizes of DeepSeek-R1-Distill-Qwen.

L2M-CoT consistently improves performance across all models and datasets, with stronger LLMs yielding greater gains in VLM reasoning ability after transfer.

D L2V-CoT Algorithm.

We propose L2V-CoT to transfer the reasoning ability of the LLM to the VLM, thereby enhancing the reasoning capability of the VLM. The detailed algorithm is shown in Algorithm S.1.

E Experimental Details

In our experiments, we inject the representations from the LLM into the VLM. Therefore, the extraction layer of the LLM, the injection strength, and the injection layer of the VLM are key hyperparameters. We divide the layers of both the LLM and VLM into three categories: low, middle, and high. Then we inject the middle-layer representations from the LLM into the VLM. The specific injection layer and strength for the VLM are shown in Table S.2 and Table S.3. The tasks in MathVista and MMStar share the same hyperparameters because they belong to the same dataset. Therefore, we use the same hyperparameters for training. In contrast, each task in MathVerse has a different training set, so

Model	MathVista			MathVerse Benchmarks					MMStar			DM	MV	
	All	General	Math	Overall	T-D	T-L	V-I	V-D	V-O	All	Percep.	Reason.		
LLAVA	12	12	12	17	16	13	14	18	19	15	15	15	17	16
InternVL	19	19	19	16	17	14	19	13	20	17	17	17	18	15
QwenVL	9	9	9	16	17	12	13	14	16	12	12	12	15	14
Idefics	15	15	15	20	19	16	14	21	12	13	13	13	16	17

Table S.2: Injection layer of the VLM.

Model	MathVista			MathVerse Benchmarks					MMStar			DM	MV	
	All	General	Math	Overall	T-D	T-L	V-I	V-D	V-O	All	Percep.	Reason.		
LLAVA	0.3	0.3	0.3	0.6	0.5	0.4	0.6	0.5	0.6	0.3	0.3	0.3	0.5	0.4
InternVL	0.4	0.4	0.3	0.7	0.6	0.3	0.7	0.4	0.6	0.6	0.6	0.6	0.5	0.6
QwenVL	0.3	0.3	0.3	0.5	0.5	0.3	0.4	0.5	0.6	0.5	0.5	0.5	0.4	0.4
Idefics	0.5	0.5	0.5	0.8	0.6	0.5	0.4	0.7	0.3	0.6	0.6	0.6	0.5	0.5

Table S.3: Injection strength.

Algorithm S.1: L2V-CoT for transfering the reasoning apability of LLM to VLM.

Input: A set of reasoning problems $\{q_i\}_{i=1}^n$, a reasoning-capable LLM M_{LLM} , a vanilla VLM M_{VLM} , A pair of question transfer template $\mathcal{T}_{\text{CoT}}^+$ and $\mathcal{T}_{\text{CoT}}^-$.

- 1: Use \mathcal{T}^+ CoT and \mathcal{T}^- CoT to convert q_i into question sets $\{q_i^+\}_{i=1}^n$ and $\{q_i^-\}_{i=1}^n$
- 2: Use $\{q_i^+\}_{i=1}^n$ and $\{q_i^-\}_{i=1}^n$ to obtain CoT responses $\{c_i\}_{i=1}^n$ and direction responses $\{d_i\}_{i=1}^n$ from M_{LLM}
- 3: Use $\{c_i\}_{i=1}^n$ and $\{d_i\}_{i=1}^n$ to extract CoT representations $h_L(c_i, l_L)$ and non-CoT representations $h_L(d_i, l_L)$ from the M_{LLM}
- 4: Construct CoT direction representations $\{u_i(l_L)\}_{i=1}^n = \{h_L(c_i, l_L) - h_L(d_i, l_L)\}_{i=1}^n$
- 5: $v(l_L) \leftarrow \text{Mean}(\{u_i(l_L)\}_{i=1}^n)$
- 6: $v_{LPF}(l_L) \leftarrow LPF(V(l_L))$
- 7: $\hat{v}_{LPF}(l_L) \leftarrow v_{LPF}(l_L)$
- 8: $h_V(l_V) \leftarrow \hat{v}_{LPF}(l_L) + h_V(l_V)$
- 9: $\hat{h}_V(l_V) \leftarrow \text{Normalize}(h_V(l_V))$
- 10: replace $h_V(l_V)$ in M_{VLM} with $\hat{h}_V(l_V)$

Model	Huggingface Checkpoint
LLaVA-Next-LLaMA3-8B	llava-hf/llama3-llava-next-8b-hf
InternVL2-8B	OpenGVLab/InternVL2-8B
Qwen2-VL-7B-Instruc	Qwen/Qwen2-VL-7B-Instruct
Idefics2-8B	HuggingFaceM4/idefics2-8b
InternVL2-26B	HuggingFaceM4/idefics2-26b
InternVL2-40B	HuggingFaceM4/idefics2-40b
DeepSeek-R1-Distill-Qwen-32	deepseek-ai/DeepSeek-R1-Distill-Qwen-32B

Table S.4: All the Huggingface checkpoints used in our experiments.

we use different hyperparameters accordingly.

We show all the checkpoints we use for experiments in Table S.4.

F Dataset Details

MathVista (Lu et al. 2023): This dataset is designed to evaluate the performance of vision-language models on multimodal math problem solving. We conduct our experiments on MathVista MINI, a subset of the full MathVista dataset. MathVista MINI is mainly used for quick experiments or training under limited resources. It contains around 1,000 questions selected from the full MathVista dataset. The questions are divided into two categories: General and Math.

MathVerse (Zhang et al. 2024): MathVerse is a large-scale benchmark for multimodal mathematical reasoning.

soning. It consists of multiple datasets from different sources, including MathQA+Draw, GSM8K+Diagrams, and SVAMP+Tables. The tasks cover various types of reasoning, such as arithmetic, algebraic, and logical reasoning, all paired with visual elements. The goal is to provide a unified evaluation of multimodal LLMs on different types of mathematical problems. Each subset can be used as an individual task dataset, which helps analyze the challenges of different question types. The tasks are categorized into six types: V-I (vision intensive), V-D (vision dominant), V-O (vision only), T-D (text dominant), T-L (text lite), and T-O (text only).

MMStar (Chen et al. 2024a): MMStar is a comprehensive multimodal math dataset. Its questions are usually closer to real-life scenarios and have longer descriptions. The dataset requires models to have basic commonsense reasoning and strong language understanding. The tasks are divided into perception tasks and reasoning tasks.

Dynamath (Zou et al. 2024): It is a dataset designed to evaluate multimodal dynamic math reasoning ability. It combines visual understanding, temporal reasoning, and mathematical modeling. The model needs to perform image modeling across time and demonstrate reasoning and memory abilities.

MathVision (Wang et al. 2024a): MathVision is a multimodal reasoning dataset focused on visual math problems. It

evaluates the model’s ability to combine image understanding with mathematical reasoning. The model needs to understand text, recognize objects in images, read chart data, and interpret visual relationships.

G Experiment Platform

We conduct comprehensive experiments utilizing the NVIDIA H800 80GB PCIe paired with the Intel(R) Xeon(R) Platinum 8380 CPU @ 2.30GHz.

H Case Study

In this section, we present several examples from n LLaVA-Next-LLaMA3-8B to intuitively demonstrate that our method can enhance the reasoning capability of VLMs. The case study examples are show in Figure S.2, Figure S.3 and Figure S.4. We can observe that our method indeed improves the reasoning ability of VLMs.

Question

Associated Image

Sample A

Mass of each particle: 44 u
Average particle speed: 1,400 m/s

Sample B

Mass of each particle: 46 u
Average particle speed: 1,400 m/s

Question: The diagrams below show two pure samples of gas in identical closed, rigid containers. Each colored ball represents one gas particle. Both samples have the same number of particles. Compare the average kinetic energies of the particles in each sample. Which sample has the higher temperature?

Choices:

- (A) neither; the samples have the same temperature
- (B) sample B
- (C) sample A

Answer: sample B

Vanilla VLM Answer

The correct answer is \boxed{(C)}. The sample A has a higher average particle speed, which indicates a higher temperature. The average particle speed is a measure of the average velocity of the particles in a gas, and it is directly related to the temperature of the gas. The higher the average particle speed, the higher the temperature. In this case, sample A has a higher average particle speed, so it has a higher temperature.



L2V-CoT Answer

The image shows two samples of gas particles, with green particles representing one type of gas and blue particles representing another type of gas. The particles are depicted as moving, with the green particles having a wavy motion and the blue particles having a straight-line motion. The wavy motion of the green particles suggests that they are moving faster than the blue particles, which are moving in straight lines. This indicates that the green particles have a higher average kinetic energy than the blue particles.

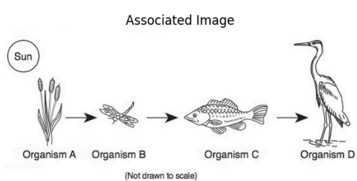
Since the samples have the same number of particles, the higher average kinetic energy of the green particles means that they are moving at a higher speed. Therefore, the sample with the green particles, which is Sample A, has a higher temperature than Sample B.

The correct answer is:
\boxed{(B)}



Figure S.2: An example of L2V-CoT transferring reasoning ability from LLM to VLM. Vanilla VLMs first give the answer and then provide an explanation. In contrast, L2V-CoT reasons for a longer time before producing the answer.

Question



Question:Question:

What would happen to organism c if organism b increased?

Choices:

- (A) decrease
- (B) increase
- (C) can't predict
- (D) stay same

Answer: increase

A

Vanilla VLM Answer



L2V-CoT Answer

The image depicts a diagram illustrating the process of natural selection, where a population of organisms (A) is exposed to a certain environmental condition (Sun), which affects the survival and reproduction of the organisms. The diagram shows three stages of the process:

1. Organism A (a plant) is shown at the beginning, with a certain number of individuals.
2. Organism B (a fish) is shown next, with a certain number of individuals.
3. Organism C (a bird) is shown at the end, with a certain number of individuals.

The arrows between the organisms indicate the direction of the process, with the number of individuals decreasing for Organism A and increasing for Organism B and Organism C.

Now, the question asks what would happen to organism C if organism B increased. To answer this, we need to consider the relationship between the organisms in the diagram and how an increase in organism B would affect organism C.

From the diagram, we can see that an increase in organism B would lead to an increase in the number of prey for organism C. This would mean that organism C would have more food available, which would lead to an increase in the population of organism C. Therefore, the correct answer is:

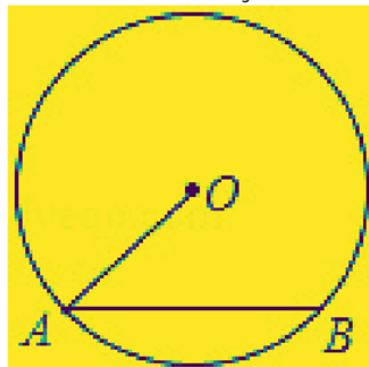
\boxed{(B)} increase



Figure S.3: An example of L2V-CoT transferring reasoning ability from LLM to VLM. The vanilla VLM tends to answer immediately. L2V-CoT, however, answers after performing extended reasoning.

Question

Associated Image



Question: As shown in the figure, it is known that the radius of $\odot O$ is 5.0 and the chord $AB = 8.0$, then the distance from the center O to AB is ()

Choices:

- (A) 1mm
- (B) 2mm
- (C) 3mm
- (D) 4mm

Answer: 3mm

Vanilla VLM Answer

The distance from the center of a circle to a chord is half the length of the chord. Therefore, the distance from the center O to the chord AB is $8.0 / 2 = 4.0$ mm. The correct answer is:

\boxed{(D)}

**L2V-CoT Answer**

To find the distance from the center of the circle to the midpoint of the chord AB , we can use the Pythagorean theorem. The radius of the circle is 5.0, and the length of the chord is 8.0. The distance from the center to the midpoint of the chord is the hypotenuse of a right triangle with sides of length 5.0 and 8.0.

Using the Pythagorean theorem, we can calculate the distance from the center to the midpoint of the chord: $c^2 = a^2 + b^2$

where c is the distance from the center to the midpoint of the chord, a is the radius of the circle (5.0), and b is the length of the chord (8.0).

$$c^2 = 5.0^2 + 8.0^2$$

$$c^2 = 25 + 64$$

$$c^2 = 89$$

$$c = \sqrt{89}$$

The distance from the center to the midpoint of the chord is approximately 9.43. Since the image shows the distance from the center to the midpoint of the chord, the correct answer is:

\boxed{(C)}



Figure S.4: An example of L2V-CoT transferring reasoning ability from LLM to VLM. It can be seen that vanilla VLMs perform short reasoning. In contrast, L2V-CoT generates the answer after a longer reasoning process.